Protein Science (1994), *3*:1651-1669. Cambridge University Press. Printed in the USA.

INVITED PAPER, SPECIAL SECTION IN HONOR OF MAX PERUTZ

Role and mechanism of the maturation cleavage of VP0 in poliovirus assembly: Structure of the empty capsid assembly intermediate at 2.9 Å resolution

R. BASAVAPPA,[1] R. SYED,[2,4] O. FLORE,[2,5] J.P. ICENOGLE,[2,6] D.J. FILMAN,[1] AND J.M. HOGLE[1,3]

[1] Department of Biological Chemistry and Molecular Pharmacology, Harvard Medical School, Boston, Massachusetts 02115
[2] Department of Molecular Biology, The Scripps Research Institute, La Jolla, California 92037
[3] Committee for Higher Degrees in Biophysics, Harvard University, Cambridge, Massachusetts 02138

(RECEIVED July 1, 1994; ACCEPTED July 28, 1994)

Abstract

The crystal structure of the P1/Mahoney poliovirus empty capsid has been determined at 2.9 Å resolution. The empty capsids differ from mature virions in that they lack the viral RNA and have yet to undergo a stabilizing maturation cleavage of VP0 to yield the mature capsid proteins VP4 and VP2. The outer surface and the bulk of the protein shell are very similar to those of the mature virion. The major differences between the 2 structures are focused in a network formed by the N-terminal extensions of the capsid proteins on the inner surface of the shell. In the empty capsids, the entire N-terminal extension of VP1, as well as portions corresponding to VP4 and the N-terminal extension of VP2, are disordered, and many stabilizing interactions that are present in the mature virion are missing. In the empty capsid, the VP0 scissile bond is located some 20 Å away from the positions in the mature virion of the termini generated by VP0 cleavage. The scissile bond is located on the rim of a trefoil-shaped depression in the inner surface of the shell that is highly reminiscent of an RNA binding site in bean pod mottle virus. The structure suggests plausible (and ultimately testable) models for the initiation of encapsidation, for the RNA-dependent autocatalytic cleavage of VP0, and for the role of the cleavage in establishing the ordered N-terminal network and in generating stable virions.

Keywords: capsid proteins; empty capsid; encapsidation initiation; maturation cleavage; poliovirus; viral RNA; virion stability

Poliovirus is a member of the picornavirus family. This family includes a large number of related small spherical viruses consisting entirely of a protein shell (approximately 300 Å in diameter) and a single-stranded RNA genome (~7,500 nucleotides) of positive polarity. The family is subdivided into several genera, including the enteroviruses (polioviruses, coxsackieviruses, echoviruses), the rhinoviruses, the cardioviruses (EMC, Mengo and Theiler's encephalomyocarditis virus), the aphthoviruses (foot-and-mouth disease virus), and hepatitis A virus. The capsid of polio and other picornaviruses consist of 60 copies each of 4 capsid proteins VP1, VP2, VP3, and VP4, arranged symmetrically on an icosahedral lattice. VP1, VP2, and VP3 are all similar in size (ca. 30 kDa), whereas VP4 is much smaller (ca. 7.5 kDa). The emergence of poliomyelitis as an epidemic disease made poliovirus and related picornaviruses the focus of considerable attention. As a result, these viruses have become paradigms for understanding simple viruses at the molecular level.

One area that has received particular attention has been how these viruses self-assemble efficiently in the course of their nat-

Reprint requests to: J.M. Hogle, Department of Biological Chemistry and Molecular Pharmacology, Harvard Medical School, 240 Longwood Avenue, Boston, Massachusetts 02115; e-mail: hogle@hogles.med.harvard.edu.
[4] Present address: Amgen Corporation, Thousand Oaks, California.
[5] Present address: University of Cagliari, Cagliari, Italy.
[6] Present address: Division of Viral Diseases, Centers for Disease Control, Atlanta, Georgia 30333.

ural infectious cycles. In the infected cell, the poliovirus genome is translated in a single large open reading frame to yield a polyprotein of approximately 200 kDa. The polyprotein is processed subsequently in a cascade of proteolytic cleavages to yield the individual viral proteins (Pallansch et al., 1984). The series of proteolytic steps involved in releasing the individual capsid proteins begins when an early cleavage of the polyprotein releases an ~100-kDa protein, P1, from the N-terminus of the polyprotein. P1 contains all the sequences corresponding to the capsid proteins. P1 is cleaved twice by viral proteases to yield the capsid proteins, VP1 and VP3, and an immature capsid protein precursor, VP0. Very late in infection, VP0 is cleaved to yield the capsid proteins, VP2 and VP4 (Holland & Kiehn, 1968; Jacobson & Baltimore, 1970). This final "maturation" cleavage is thought to be autocatalytic (Hogle et al., 1985; Rossmann et al., 1985).

A number of intermediates accumulate to significant levels in the course of poliovirus assembly. These include the protomer consisting of P1; a cleaved protomer containing 1 copy each of VP0, VP1, and VP3; the pentamer, consisting of 5 copies each of VP0, VP3, and VP1 (Watanabe et al., 1965; Phillips & Fennel, 1973); the empty capsid, consisting of 60 copies each of VP0, VP3, and VP1 (12 pentamers) (Jacobson & Baltimore, 1968a); and the mature virion, consisting of 60 copies each of VP1, VP2, VP3, and VP4 and the viral RNA. Some early studies have reported an additional intermediate termed the provirion, consisting of 60 copies each of VP0, VP1, and VP3, and 1 copy of the viral RNA (Fernandez-Tomas & Baltimore, 1973; Guttman & Baltimore, 1977). The assembly process is intimately linked with the series of proteolytic processing steps. Thus, cleavage of P1 to yield VP0, VP3, and VP1 is a prerequisite for the formation of the pentameric assembly intermediate (Palmenberg, 1982, 1990). Similarly, cleavage of VP0 does not occur until very late in assembly and is associated with the encapsidation of the viral RNA.

There is considerable controversy concerning the role of empty capsids and provirions in the assembly process. Pulse-chase experiments are consistent with a pathway in which protomers assemble into pentamers, which subsequently assemble into intact shells including empty capsids, provirions, and virions (Phillips et al., 1968; Jacobson & Baltimore, 1970; Oppermann & Koch, 1973), but the exact kinetic roles of the empty capsids and provirions have not been established. Thus, it is unclear whether the viral RNA is inserted into empty capsids (Jacobson & Baltimore, 1968a) (analogous to the insertion of DNA into bacteriophage proheads) or whether the RNA is encapsidated by the condensation of pentamers around it (Ghendon et al., 1972) (analogous to encapsidation in small plant viruses). In the latter case, the empty capsids may function as a reserve form of pentamers in which proteolytically sensitive areas are protected but from which the pentamers still can dissociate to condense around the viral genome. The relevance of the provirion to the assembly process is even less certain. Early observations of the provirion suggested that it was the immediate precursor of the mature virion (Fernandez-Tomas & Baltimore, 1973). However, these observations of the provirion in wild-type poliovirus infections have been difficult to reproduce, leading a number of investigators to question its role. Recently, Compton et al. (1990) described a temperature-sensitive mutant of P1/Mahoney poliovirus that accumulates provirion-like particles at the nonpermissive temperature. However, it is not clear whether these particles are actual intermediates or are dead-end products in the assembly pathway. Regardless of the role of these intermediates, it is clear that particles in which VP0 is uncleaved are much less stable than mature virions to a variety of conditions, including elevated temperature, detergents, high salt, and extremes of pH (Guttman & Baltimore, 1977). This suggests that VP0 cleavage may be required for the production of stable particles.

The 3-dimensional structures of several poliovirus and of several related picornaviruses have been determined at near atomic resolution by X-ray crystallographic methods (Hogle et al., 1985; Rossmann et al., 1985; Luo et al., 1987, 1992; Acharya et al., 1988; Grant et al., 1992). These studies have shown that the major capsid proteins VP1, VP2, and VP3 share a common "core" structure, composed of a wedge-shaped 8-stranded antiparallel β-barrel, but have dissimilar connecting loops, and long dissimilar extensions at their amino-termini. The cores pack to form the closed shell of the virion, with the narrow end of VP1 pointing toward the 5-fold axes and the narrow ends of VP2 and VP3 alternating around the 3-fold axes. The connecting loops decorate the outer surface of the virion and contain the antigenic sites. The N-terminal extensions, together with VP4, form an elaborate network that decorates the inner surface of the protein shell.

The picornavirus crystal structures have provided considerable insight into the role of proteolytic processing of P1 in the assembly of pentamers (Arnold et al., 1987; Flore et al., 1990). The structures have provided less information about the late stages of assembly. In the mature virion, the C-terminus of VP4 and the N-terminus of VP2 that are released by the cleavage of the precursor protein VP0 are found close to each other in the structure of the mature virion. In both poliovirus and rhinovirus, structural studies revealed a hydrogen bond between the C-terminal carboxylate groups of VP4 and the side-chain hydroxyl group of Ser 10 of VP2. This observation prompted the suggestion of a serine protease-type mechanism for the cleavage, in which the hydroxyl group of Ser 10 of VP2 served as the nucleophile and one of the nucleotide bases of the viral RNA served as the base (in place of histidine) in the now-classic catalytic triad (Arnold et al., 1987). However, introduction of a mutation in which Ser 10 of VP2 is replaced by Ala does not interfere with VP0 cleavage (Harbor et al., 1991). Thus, both the mechanism of VP0 cleavage and the role of this cleavage in generating stable particles remain unknown.

In order to address these issues, we have undertaken structural studies of the empty capsid assembly intermediate. Although the empty capsids accumulate to levels that are readily detectable using radiolabels, the levels normally found within infected cells are too low to support crystallographic studies. However, in the presence of millimolar levels of guanidine-HCl (a specific inhibitor of poliovirus RNA replication), empty capsids accumulate to very high levels due to the unavailability of genomic RNA (Jacobson & Baltimore, 1968b). Like the naturally occurring empty capsids, the empty capsids that accumulate in the presence of guanidine are fully dissociable to

pentamers upon exposure to mildly alkaline conditions and are indistinguishable from mature virions using a variety of immunological probes (Icenogle et al., 1981; Marongiu et al., 1981; Rombaut et al., 1982). Moreover, like the naturally occurring empty capsids, these particles are very labile and cannot be purified by the protocols used to prepare mature virions. We have developed a fast and very efficient procedure for preparing large amounts of very pure empty capsids. We report here the 3-dimensional structure of this intermediate at 2.9 Å resolution and discuss its relevance to the mechanism and role of VP0 cleavage (Kinemage 1).

Results

The purification protocol reported here replaces an earlier protocol in which the empty capsids were purified using polyethyleneglycol (PEG) precipitation and multiple fractionations on sucrose gradients (O. Flore & J.P. Icenogle, unpubl.). This earlier protocol produced material whose purity varied from preparation to preparation. However, several preparations did yield material that produced diffraction-quality crystals. Diffraction data were collected from these crystals, and a preliminary structure was determined (R. Syed, D.J. Filman, & J.M. Hogle, unpubl.). However, the highly variable purity of the material and consequent variable quality of the crystals resulted in data of very marginal quality. The revised purification protocol (described in the Materials and methods) eliminates the PEG precipitation step and replaces the multiple sucrose gradients with a single sucrose gradient and an equilibrium buoyant density fractionation on a self-forming Nycodenz density gradient. Nycodenz is a triiodobenzene derivative originally used as a contrast agent in medical imaging. Like CsCl, uniform solutions of Nycodenz spontaneously form density gradients spanning the density of many biological macromolecules when subjected to high centrifugal fields (Rickwood, 1983). Unlike CsCl, however, Nycodenz is nonionic and remains soluble at low temperatures such as 4 °C. Thus, it provides a useful (and more gentle) alternative to CsCl for biological samples, such as the empty capsids, that are sensitive to high ionic strength and to prolonged exposure to ambient temperatures. The revised procedure yields highly purified samples of the empty capsids that reproducibly provide high-quality crystals for diffraction analysis. In the protocol described here, the Nycodenz gradient is run first (Fig. 1A), followed by the sucrose gradient (Fig. 1B). However, the order of the 2 steps does not appear to be important (data not shown). The material produced is estimated to be greater than 98% pure by SDS-PAGE (Fig. 1C), and it is better than 95% dissociable to pentamers upon exposure to basic pH (Fig. 1D).

A 3-dimensional set of X-ray diffraction data was assembled from 51 half-degree oscillation photographs collected from 22 crystals. Statistics for the final merged data set are presented in Table 1. Although this data set is incomplete (61.7% complete overall, 55.8% complete in the outermost resolution shell [2.97–2.88 Å]), the 30-fold noncrystallographic redundancy results in the data being heavily oversampled with respect to the noncrystallographic unique volume.

The structure was determined by the molecular replacement technique using the refined model of the mature P1/Mahoney poliovirion as the initial phasing model. The empty capsid crystals are nearly isomorphous with those of the mature virion, suggesting that the orientation and position of the icosahedral particle would be very similar in the 2 crystals. In both crystal forms, packing considerations dictate that the particle must be oriented such that one of its 2-fold axes is coincident with the crystallographic 2-fold (the *c* axis), and the observation of systematically weak intensities for all odd-ordered reflections indicates that the particle is positioned approximately at $z = 1/4$ with 2-fold axes nearly parallel to the crystallographic *a* and *b* axes. The orientation and position were refined by a trial search procedure that systematically sampled the orientation of the particle about the *z* axis and the translation along the *z* axis in the vicinity of the corresponding parameters for the mature virions. The refined orientation and position of the particle in the empty capsid crystals ($z = -0.24974$ and rotation of 2.162° about *c*) were not significantly different from the corresponding parameters for the mature virions.

Table 1. *Statistics of the P1/Mahoney empty capsid data set*

Crystals (no.)	22
Films (no.)	51
Measurements (no.)	1,885,617
Unique *hkl* measured (no.)	610,509
Unique *hkl* used (no.)	607,564
R_{sym}[a] (all measurements ≥50%)	0.189
R_{sym}[a] (fully recorded measurements)	0.149

[a] R_{sym} is an index of the self-consistency of multiply-measured reflections. It is defined as the normalized sum of the absolute differences of multiply-measured reflections ($I_{\mathbf{h}j}$) from their σ-weighted mean ($\langle I_{\mathbf{h}} \rangle$).

$$R_{sym} = \sum_{\mathbf{h}} \sum_{j} |I_{\mathbf{h}j} - \langle I_{\mathbf{h}} \rangle| \Big/ \sum_{\mathbf{h}} \sum_{j} \langle I_{\mathbf{h}} \rangle .$$

To assess the differences between the empty capsid structure and that of the mature virion a difference electron density map was calculated using coefficients of the form $(|F_{empty}| - |F_{mature}|)\exp(i\alpha_{mature})$, where $|F_{empty}|$ are the observed amplitudes for the empty capsids and $|F_{mature}|$ and α_{mature} are the amplitudes and phases obtained by Fourier transformation of the icosahedrally averaged electron density of the mature virions. Inspection of this difference map indicated that, in most of the structure, the empty capsid and mature virions are very similar. However, there were very significant difference density features in specific areas of the map. These major difference density features were located on the inner surface of the capsid in areas corresponding to the location of residues VP1: 1-68; VP2: 5-9, 10-25, 44-57; VP3: 158-162; and VP4: 9-16, 23, 24, 45-69 in the mature virus.

In order to minimize potential phase bias in the molecular-replacement structure determination, all residues of the capsid proteins that were associated with significant difference electron density were removed from the model used to derive initial phase estimates. This initial phasing model was refined to convergence using the noncrystallographic symmetry-based phase constraint procedure of Bricogne (1974). The overall quality of the resulting icosahedrally averaged electron density map was excellent. The map provided interpretable density throughout most of the

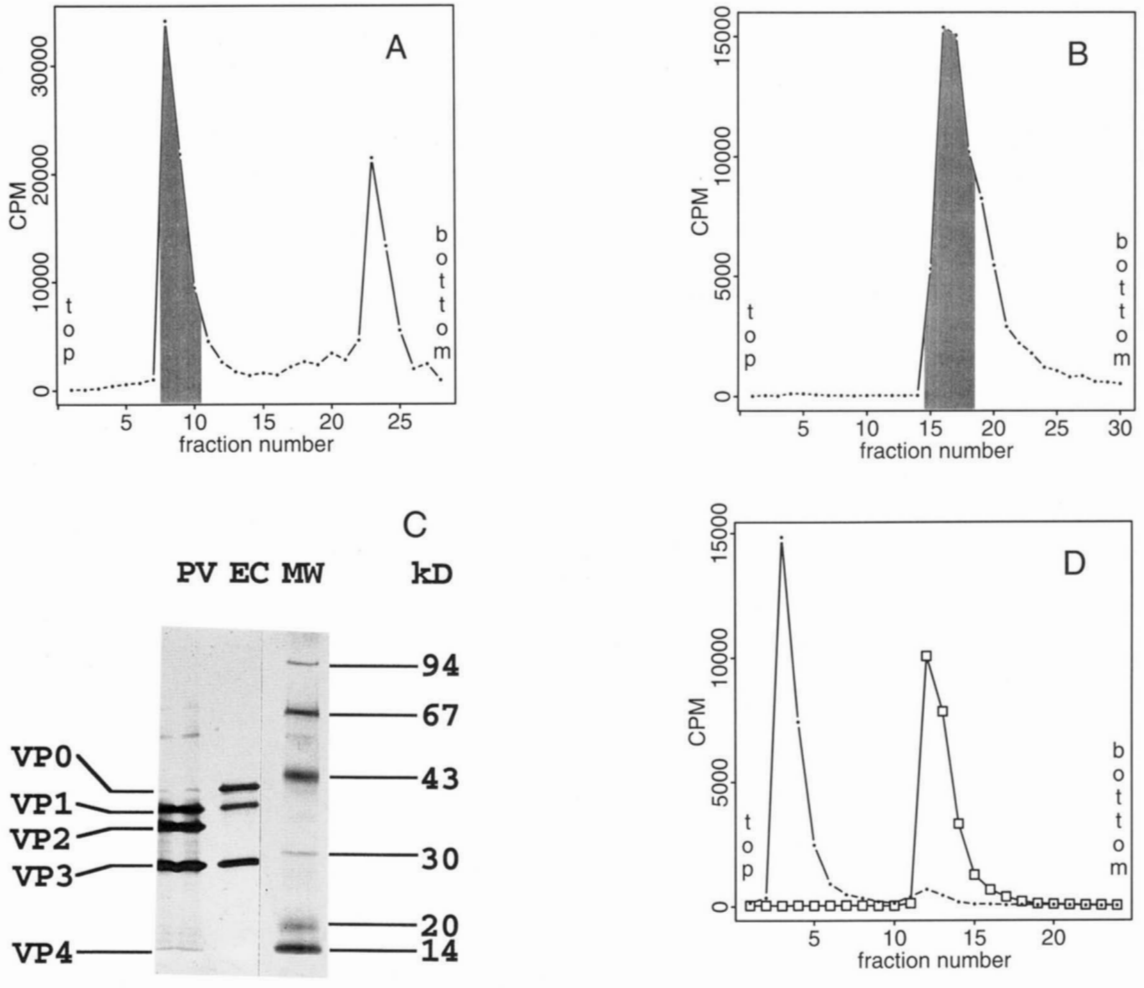

Fig. 1. Summary of the empty capsid purification procedure. **A:** Buoyant density separation in a self-forming Nycodenz gradient. The gradient was fractionated, and an aliquot from each fraction was counted for radioactivity. The shaded area corresponds to pooled fractions. The smaller peak corresponds to mature virus. **B:** Rate-zonal separation in a preformed 15–30% sucrose gradient. This purification step is performed after the separation in Nycodenz. **C:** Purity, as assessed by SDS-PAGE analysis, of the empty capsid sample obtained by the above procedure. PV, EC, and MW denote mature poliovirus, empty capsid, and molecular weight standards, respectively. **D:** Dissociability of the purified empty capsids upon treatment with moderately alkaline pH (~8.4). Such treatment will dissociate native empty capsids but not non-native (H-antigenic) empty capsids. The plot shows sedimentation of alkaline-treated empty capsids (dots) in 15–30% sucrose gradient. Dissociated empty capsids will sediment as pentamers near the top of the gradient. A control of untreated empty capsids (squares) run in parallel shows sedimentation of intact empty capsids.

capsid proteins, including several regions where the structure differed significantly from that observed in the mature virion. In particular, there was a significant density feature on the inner surface of the empty capsids that was interpreted to represent a stretch of peptide spanning the scissile bond of VP0. Although the position and conformation of this polypeptide segment differed significantly from those of the termini released by VP0 cleavage in the mature virions, the density was completely consistent with the sequence for some 10 residues on either side of the scissile bond. In contrast, the map provided no interpretable density for residues in the N-terminal extension of VP1, for residues corresponding to the central region of VP4 (residues 45–56), and for 2 segments in VP0 corresponding to the N-terminal extension of VP2 in the mature virion (residues 10–12, 45–57). Given the excellent overall quality of the map (Fig. 2), the absence of electron density for these segments probably reflects inherent disorder in these regions of the proteins in the empty capsids.

A complete atomic model for all ordered portions of the empty capsids was built into this map and the model was refined by alternating cycles of pseudo-real-space refinement, application of noncrystallographic symmetry constraints, and manual rebuilding. In the final stages of refinement, the pseudo-real-space procedure was replaced by a novel method in which changes in the atomic positions and temperature factors are derived by combining the gradient of a crystallographic residual (evaluated over a box encompassing the icosahedral unique volume) with the gradient of a stereochemical potential provided by the X-PLOR (Brünger, 1992) program. Statistics for the final refined model are summarized in Table 2.

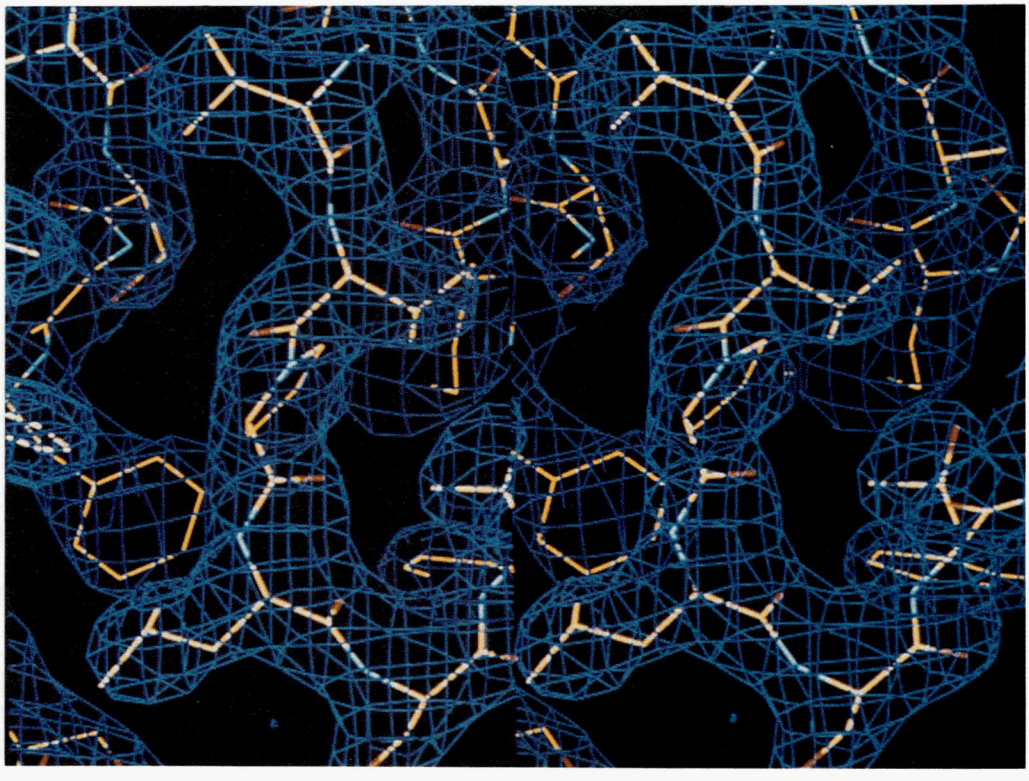

Fig. 2. View of electron density corresponding to a well-ordered region of the empty capsid. The electron density shown was obtained by the application of phase constraints afforded by the 30-fold noncrystallographic symmetry. This figure was prepared using the program FRODO (Jones, 1985).

Comparison of the structures of the empty capsids and mature virions

Pairwise differences in α-carbon position between the polypeptides in the empty capsids and the mature virus are summarized in Figure 3. The 3-dimensional folds of the polypeptides are compared in Figure 4. As expected, the overall architectures of the empty capsid and the mature virus are very similar. The β-barrel structures in the empty capsid particle are virtually indistinguishable from their counterparts in the mature virion (Figs. 3, 4). The RMS deviation between the positions of corresponding α-carbons in the β-barrels of the 2 particles is 0.43 Å, with none of the deviations exceeding 1.0 Å. Indeed, viewed from outside, the particles are remarkably alike (Fig. 3). The α-carbons of residues in the loops that are exposed on the outer surface and in the C-termini of VP0/VP2, VP1, and VP3 (also on the outer surface) have an RMS deviation in position of 0.41 Å. This similarity in the outer surface is consistent with previous demonstrations that the empty capsids and mature virions are immunologically indistinguishable. The only significant differences (>1 Å) in the outer surface occur at residues 171, 233, and 244 of VP1 and the C-terminus of VP3. Residue VP1:171 is located about half-way up the peak centered at the 5-fold axis of the pentamer, whereas residues VP1:233 and VP1:244 are near the canyon that surrounds this 5-fold peak. In all 3 cases, the deviation in α-carbon position with respect to the mature virus is slightly more than 1 Å. In none of these 3 cases does the difference seem to have any functional import. However, the difference at the C-terminus of VP3 is more intriguing. In the case of the mature virus, the electron density for the VP3 chain stops abruptly after residue 235, consistent with this being the C-terminal residue. In the case of the empty capsid, however, the electron density clearly continues past this residue. Three residues (numbered 236–238 and modeled as Ala-Ala-Gln) have been built convincingly into this extended density. These residues arch over the canyon so that the VP3 terminal residue of 1 protomer interacts with residues from the same protomer and from symmetry-related protomers in the 5-fold peak of the pentamer. Because the sites in the empty capsid occupied by these residues are identical to those in the mature virus, there is no clear indication of why the residues would not be ordered in the mature virus if they were present. It is possible that these 3 residues are removed in the productive assembly process, but the occurrence of such a cleavage has yet to be confirmed.

Differences in the internal network

Unlike the other regions of the shell, the inner surface is dramatically different in the 2 particles (Fig. 3). The major differences can be classified into 2 general categories. The first category of differences includes several peptide segments that are well ordered in the mature virion but disordered in the empty capsids. These include the entire N-terminal extension of VP1

Table 2. *Statistics for the current model of P1/Mahoney empty capsid*[a]

Resolution shell (Å)	Unique *hkl* used	% Total shell	R_1 model[b]	R_1 non-x symm.[c]	R_{corr} non-x symm.[d]
11.51	8,691	53.5	0.4401	0.1086	0.9565
8.14	17,714	61.5	0.2948	0.0810	0.9826
6.65	23,099	62.5	0.3005	0.0999	0.9717
5.76	27,364	62.9	0.2615	0.1063	0.9666
5.15	30,799	62.5	0.2317	0.1098	0.9635
4.70	33,966	62.5	0.1987	0.1123	0.9610
4.35	36,911	62.6	0.1906	0.1200	0.9557
4.07	39,745	62.8	0.2028	0.1337	0.9460
3.84	41,971	62.4	0.2202	0.1503	0.9324
3.64	44,492	62.6	0.2386	0.1704	0.9159
3.47	46,787	62.7	0.2697	0.1972	0.8900
3.32	48,570	62.2	0.3023	0.2279	0.8580
3.19	50,507	62.1	0.3327	0.2608	0.8259
3.08	52,761	62.5	0.3903	0.3153	0.7682
2.97	54,519	62.2	0.4566	0.3845	0.6908
2.88	49,688	55.8	0.5138	0.4679	0.5785
Total	607,564	61.7	0.2809	0.1840	0.9326

[a] The current atomic model for P1/Mahoney empty capsid includes 6,078 non-hydrogen atoms representing the protein, myristate, sphingosine, and 210 ordered solvent atoms. The bond distances and bond angles in the model have 0.015 Å and 2.5° RMS deviations from their ideal values, respectively. Individual isotropic temperature factors were restrained to have a target standard deviation of 1.5 Å^2 for bonded main-chain atoms and 2.0 Å^2 for bonded side-chain atoms. R_1 measures the agreement between observed ($|F_o|$) and calculated ($|F_c|$) structure factors and is defined as:

$$R_1 = \frac{\sum_{\mathbf{h}} \| F_o | - | F_c \|}{\sum_{\mathbf{h}} | F_o |}.$$

[b] R_1 (model) is calculated with $|F_c|$ obtained by Fourier transformation of the atomic model.

[c] R_1 (non-x symm.) is calculated with $|F_c|$ obtained by Fourier transformation of the symmetry-averaged electron density map.

[d] R_{corr} is the linear correlation coefficient measuring the scale-independent agreement between $|F_o|$ and the $|F_c|$ obtained by Fourier transformation of the symmetry-averaged electron density map.

(residues 1–67), the central region of VP4 (residues 45–56), and portions of the N-terminal extension of VP2 (residues 45–57). The second category of differences involves residues near the scissile bond of VP0. The location and environment of these residues in the empty capsid are stunningly dissimilar to those of the corresponding residues in the mature virus (Fig. 5).

The significance of these differences is best understood in the context of the structure of the internal network that is seen in the mature virion. In the mature virus, the N-terminal extensions of VP1, VP2, and VP3, together with much of VP4, form an elaborate network that decorates the inner surface of the protein shell (Fig. 6). This network contributes to a number of significant intraprotomer, intrapentamer, and interpentamer interactions, and has been proposed to play an important role in directing assembly and in stabilizing assembly intermediates and the mature virion (Hogle et al., 1985; Flore et al., 1990). The major features of this network are: (1) A β-annulus centered on the 5-fold axis of the pentamer and formed by the intertwining of the 5 symmetry-related copies of the N-terminal regions of VP3. This annulus is flanked by 5 copies of a 3-stranded β-sheet, each copy of which contains 2 β-strands from the N-terminal region of VP4 and 1 strand from the N-terminal region of VP1. The myristoyl groups that are covalently attached to the N-termini of VP4 mediate the interaction between VP4 and the VP3 β-annulus (Fig. 7A). (2) Contacts between portions of N-terminal extensions of VP1 and VP2 from 2 different 5-fold related protomers (Fig. 7B). (3) An interpentamer 7-stranded β-sheet constructed from 4 strands in the core of VP3 (the CHEF strands), 2 strands from the N-terminal extension of VP2 from a 3-fold related pentamer, and a strand from the N-terminal extension of VP1 of the first protomer (Fig. 7C). (4) Interactions between a loop in the N-terminal extension of VP1 (residues 45–60) and the lower surfaces of the VP2 and VP3 β-barrels (Fig. 7D).

The N-terminal arm of VP1 is involved in all of these key structural features. The failure of the N-terminal extension of VP1 to form an icosahedrally ordered structure in the empty capsids, therefore, results in the absence of much of this network. The central role of the N-terminal arm of VP1 in the formation of the network is made more apparent by comparing the above-mentioned features of the network in the mature virion with their (rudimentary) counterparts in the empty capsid.

In the mature virus, residues close to the N-terminus of VP1 (tentatively identified as residues 6–10) provide one of the strands in the small 3-stranded β-sheet that flanks the VP3 annulus at the 5-fold axes (Fig. 7A). Although these residues are poorly ordered in the crystal structures of the mature virion, the complete disorder in these residues in the empty capsid is accompanied by a significant decrease in the order of the myristate group and of the 2 strands of VP4 that flank the VP3 annulus. This additional disorder in the N-terminus of VP4 is reflected in a distortion of the β-sheet geometry and a significant increase in the temperature factors of these residues in the empty capsid structure. It should be noted, however, that the β-annulus itself, which is formed by the 5 intertwining copies of the N-terminus of VP3, is intact in the empty capsids. The integrity of the β-annulus is consistent with previous suggestions that the formation of this structure drives pentamer assembly and contributes to the stability of the pentamer intermediate (Hogle et al., 1985).

In the mature virion, residues 29–34 and 62–67 of VP1 are roughly antiparallel and run along the periphery of the protomer (Fig. 7B). Residues 62–67 make extensive contacts with residues 42–52 in the N-terminal extension of VP2 from a 5-fold related protomer. Evidently, the interactions provided by VP1:62–67 contribute substantially to the stability of the neighbor because, in the empty capsid, the disorder of the VP1 segments is accompanied by significant disorder in the neighboring region of VP2. In this case, the disorder is sufficiently great that it has not been possible to build a model for residues 44–57 of VP2 in the empty capsid.

In the mature virion, residues 35–44 and 59–62 of VP1 make extensive contacts with the N-terminal region of the VP2 poly-

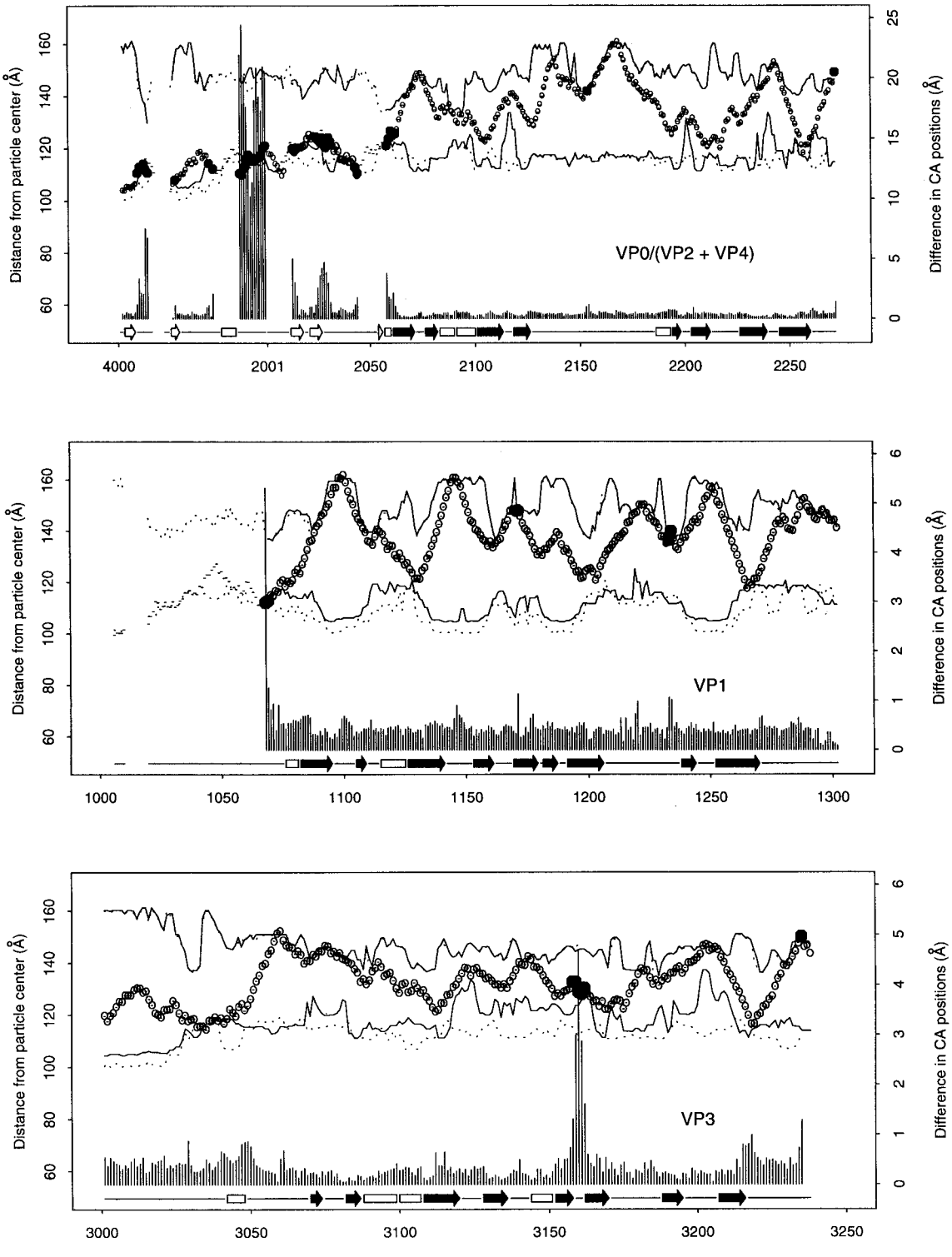

Fig. 3. Comparison of the P1/Mahoney empty capsid and mature virus structures. In all 3 panels, each residue is identified by its sequence number in the chain, preceded by its polypeptide number (e.g., 4,006 for residue 6 of VP4). The comparison of VP0 with VP2 and VP4 is shown in the top panel. Comparisons of VP1 and of VP3 are shown in the middle and bottom panels, respectively. The bar plots give pairwise differences in α-carbon position (axes on right). Below the bar plots, the positions of the secondary-structural elements in the sequence are indicated by arrows (representing β-strands) and rectangles (representing helices). The darkened arrows represent the β-strands that comprise the β-barrel cores. The diagrams above the bar plots indicate the radial positions (distance from particle center) of each α-carbon in the empty capsid (open circles) and mature virus (closed circles). The radial distance scale is given on the left axes. The larger dark circles correspond to α-carbons whose positions differ by more than 1 Å in the empty capsid and mature virus. The lines above and below the radial distance plots denote the distance of the outer and inner surfaces in the radial direction of the α-carbon (solid and dashed lines for the empty capsid and mature virus, respectively). The figure was prepared using the program SPLUS (Statistical Sciences, Inc.).

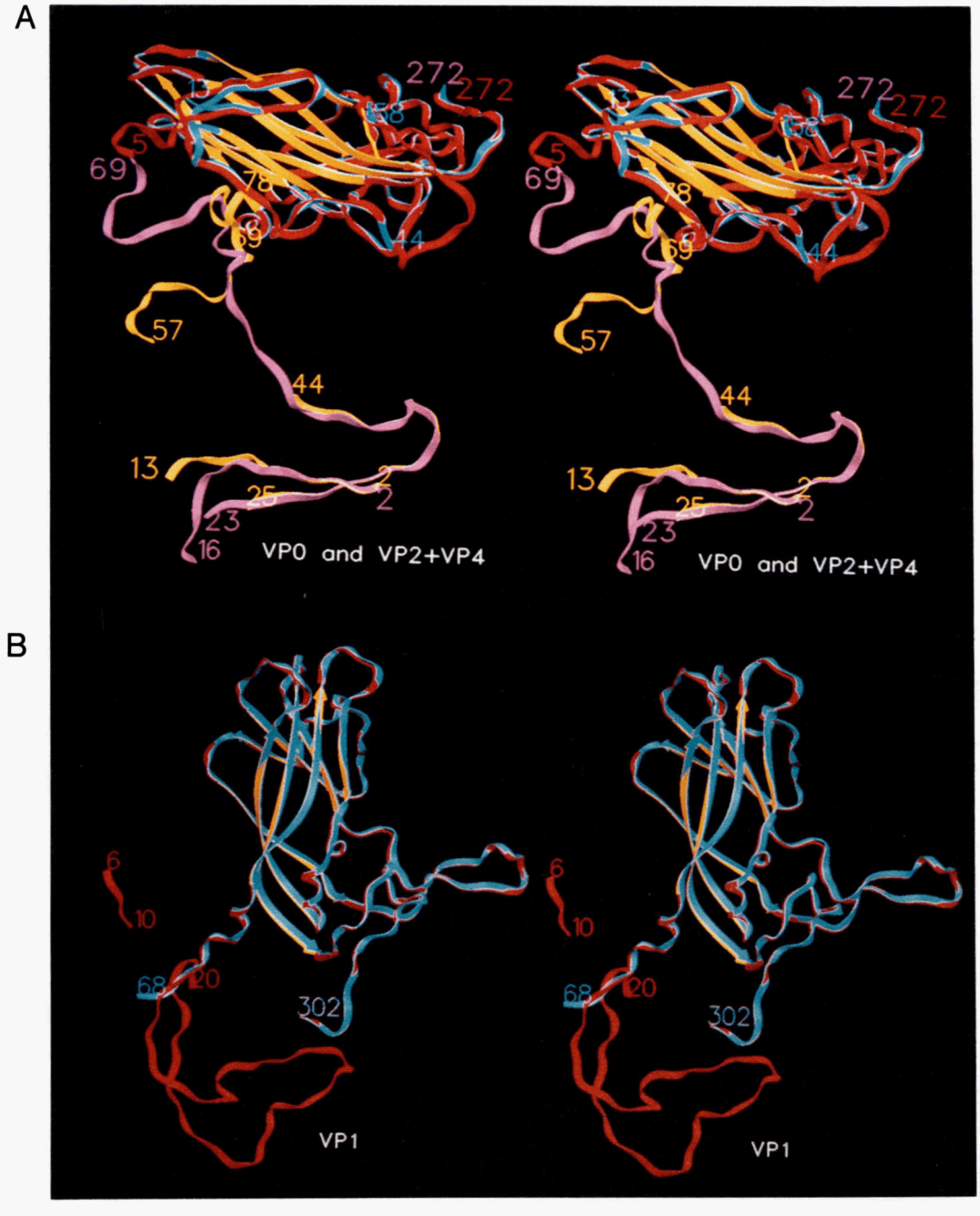

Fig. 4. Views comparing the 3-dimensional folds of the polypeptides in the empty capsid and the mature virion. Comparisons of VP0/(VP2, VP4), VP1, and VP3 are given in **(A)**, **(B)**, and **(C)**, respectively. In each of the stereo pairs, the 8 strands comprising the β-barrel are shown with arrowheads. VP1, VP2, and VP3 in the mature virion are shown in red (except for the strands of the β-barrel, which are shown in light orange). The corresponding polypeptides in the empty capsid structure are shown in blue. VP4 (in A) is shown in yellow and the corresponding segment in VP0 is shown in purple. The N- and C-termini are numbered as well as residues adjacent to disordered (unmodeled) polypeptide segments. (*Continues on facing page.*)

peptide belonging to a 3-fold related protomer (Fig. 7C). The most salient set of interactions involves a 7-stranded β-sheet formed by residues from 2 different pentamers. In this sheet, residues 36–38 in VP1 in 1 protomer form an outer strand that clamps 2 strands provided by the N-terminal extension of VP2 from a 3-fold related (interpentamer) protomer in place below the C, H, E, and F strands of the VP3 core in the first protomer. In the empty capsid, the disorder of the residues from VP1, together with steric constraints caused by the covalent attachment of VP4 and VP2, results in a significant distortion and disordering of the 2 strands of the sheet that are contributed by the residues of VP0 corresponding to residues 14–25 of VP2. The

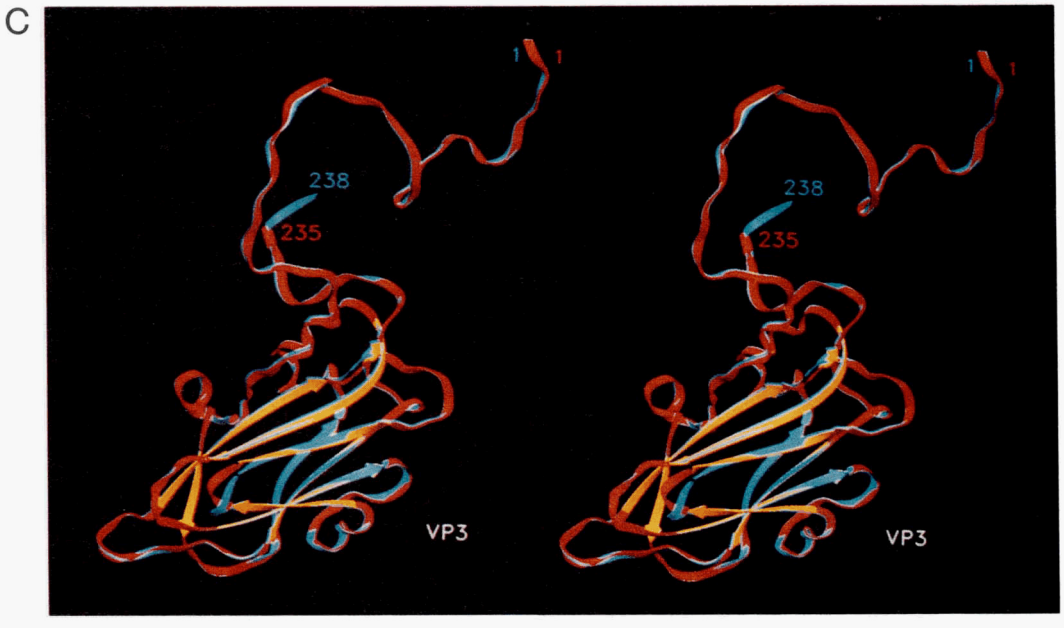

Fig. 4. *Continued.*

disorder in this region can be modeled either by high thermal mobility or by low occupancy. The temperature factors for these residues from VP0 in the empty capsids range from 50 to 60 Å^2 versus 10 to 20 Å^2 for the corresponding residues from VP2 in the mature virus. Alternatively, the occupancies for these residues in the empty capsid refine to 10–20% if the thermal parameters are held fixed to an optimum overall value. It should be noted, however, that the rudimentary presence of a mature virionlike structure for these residues is not due to contamination with low levels of mature virions because, even after prolonged storage during crystallization, the preparations contain at most 1% of VP2 (data not shown). We therefore interpret the virus-

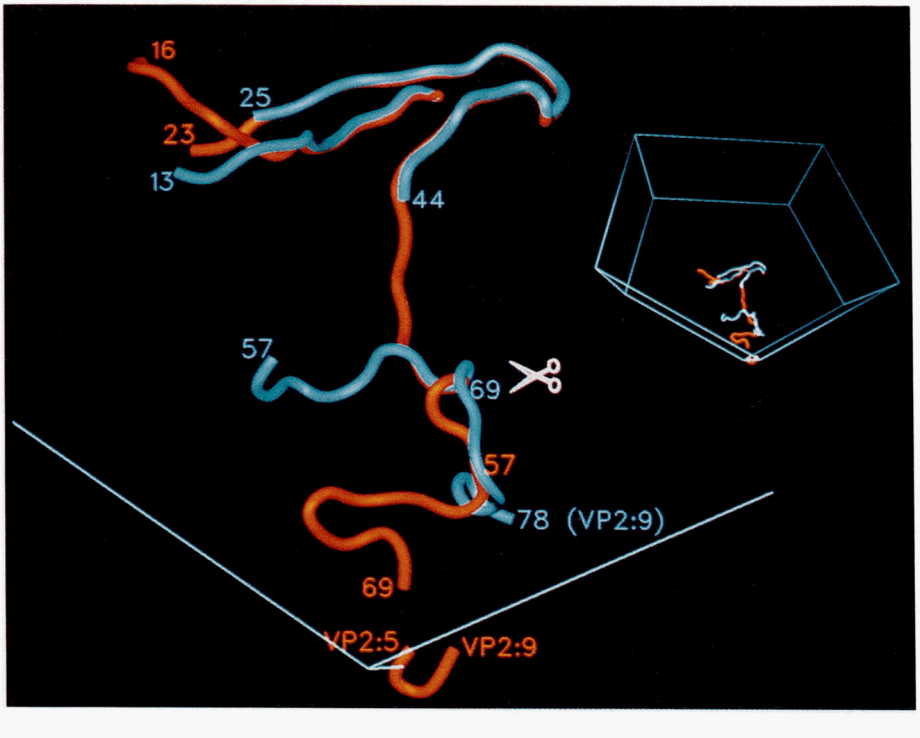

Fig. 5. Comparison of the α-carbon traces of VP4 and the region of VP2 in the mature virion (red) with the corresponding residues in the empty capsid (blue). For clarity, the trace of VP2 after residue 9 is not shown. The scissors indicate the location of the scissile bond in VP0 (between residues 69 and 70). The thin blue lines demarcate the approximate pentamer boundary. The inset shows the perspective from which the image was photographed. This figure was made using SETOR (Evans, 1993) and Showcase (Silicon Graphics, Inc.).

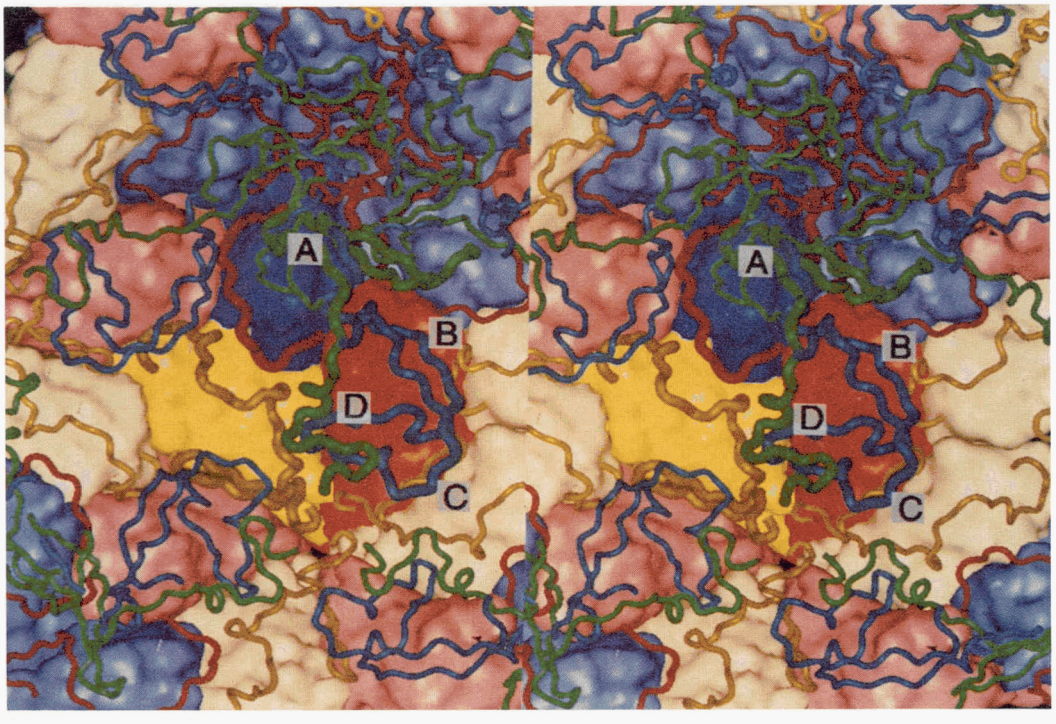

Fig. 6. Network formed on the inner surface of the mature virion by VP4 and the N-terminal extensions of VP1, VP2, and VP3 (represented as ribbons). The remaining portions of VP1, VP2, and VP3 are represented by the surfaces. VP1, VP2, VP3, and VP4 are color-coded as blue, yellow, red, and green, respectively. The bright surface colors and the thick ribbons denote the reference protomer, whereas the muted colors and thin ribbons denote symmetry-related protomers. A 5-fold symmetry axis and a 3-fold symmetry axis are in the upper and lower portions of the figure, respectively. The letters A, B, C, and D mark the significant interactions made by the N-terminal extension of VP1 and also relate to the panels of Figure 7. This image was created using InsightII (Biosym Technologies) and Smooth_Surfer (R. Basavappa, unpubl.).

like structure as an indication that these residues have a strong tendency to adopt the conformation seen in the mature virion but cannot form completely the stable structure until VP0 is cleaved.

Structural changes involving these residues (14–25 of VP2) also affect the loop connecting the F and G strands of the core of VP3 (residues 158–162). In both the mature virus and the empty capsid, the residues from the F strand of VP3 form hydrogen bonds with the 2-stranded β-sheet at the N-terminus of VP2, and in the mature virus, the FG turn interacts with the 2-stranded β-sheet in its mature conformation as well. In the empty capsids, however, the structural alterations in this region of VP0 are propagated, causing changes in the FG turn of VP3. As a consequence, although the FG turn is well-ordered in the empty capsids, its structure is very different from that observed in the mature virions (the maximum deviation in α-carbon positions is 5 Å). This constitutes the largest difference observed in the core region of the structures.

Finally, in the mature virion, residues 44–56 of VP1 and the one-third of VP4 closest to its C-terminus underlay the lower surfaces of the VP2 core and of the VP3 core from the same protomer (Fig. 7D). The disorder of these residues of VP1 and the rearrangement of the C-terminus of VP4 (see below) uncover these surfaces and create a very curious depression in the inner surface of the empty capsid. Within each protomer, the depression is shaped like a scoop. The narrow end of the scoop is near the point where VP1, VP2, and VP3 from that protomer abut (nearly 1/3 of the way along a line joining the 3-fold and the 5-fold axes) (Fig. 8). The open end of the scoop opens up onto the 3-fold axis. Two features of this depression are particularly noteworthy. First, the depression is unusually hydrophobic (especially considering that it is exposed to what is essentially an aqueous environment in the empty capsid). This suggests that the depression may serve as a site for interaction with another macromolecule. Second, the depression results in a significant thinning of the shell in the vicinity of the 3-fold axes. This suggests that interaction of a macromolecule ligand in this site might significantly enhance the stability of the VP2–VP3 interactions within a protomer. In the mature virus, the loop of VP1 plays the role of this ligand.

The position and environment of the scissile bond

The scissile bond and approximately 10 residues flanking it on either side are defined very well in the electron density map. The scissile bond is located near the center of the inner surface of the protomer and sits in a highly exposed position on the rim of the scoop-shaped depression. The position of the scissile bond is some 20 Å away from the location in the mature virus of the termini freed by its cleavage. Thus, large-scale rearrangement

of the C-terminal region of VP4 and the N-terminal region of VP2 must accompany the maturation cleavage and encapsidation of the viral RNA. It is not clear whether the cleavage of the scissile bond triggers the structural rearrangement or whether chain rearrangement potentiates cleavage of the scissile bond.

In either case, the comparison of the position of the residues near the scissile bond in the empty capsid with that of the corresponding chain termini in VP4 and VP2 immediately suggests a link between the conformational rearrangement associated with cleavage of VP0 and the ordering of at least part of the N-terminal extension of VP1. First, residues in the segment 57–61 of VP0 in the empty capsid would clash sterically with residues in VP1 near the VP1 N-terminal loop if these residues of VP1 were to occupy their positions as seen in the mature virus. Thus, the position of VP0 may prevent some segments of VP1 from assuming the structure found in the mature virus. Second, in the mature virion, residues 57–67 of VP4 fold over the N-terminal loop of VP1 (residues 44–56), holding it in place. Therefore, the cleavage and subsequent rearrangement, or the rearrangement and subsequent cleavage, may be necessary both to permit the formation of this critical loop and to stabilize the structure of the loop once it is formed.

Discussion

Role of VP0 cleavage in virion stability

One of the major goals of undertaking the determination of the empty capsid structure was to understand the basis for the significantly lower stability of the empty capsid (compared to that of the mature virus), including the role VP0 cleavage might play in determining the virus stability. Early studies with temperature-sensitive and nontemperature-sensitive variants of the Sabin vaccine strain of type 3 poliovirus pointed to 3 specific areas of the mature virus structure that appear to play a critical role in determining the stability of the virion and of assembly intermediates (Filman et al., 1989; Minor et al., 1989; Macadam et al., 1991). These sites include: (1) a pocket in the β-barrel core of VP1, (2) the interface between 5-fold related protomers, and (3) the network formed by the N-terminal extensions of the capsid proteins in the inner surface of the virion.

In the mature virion and the empty capsid, the pocket in VP1 binds a ligand that has been modeled provisionally as sphingosine. Such a ligand is present in all known structures of poliovirus and in the structures of rhinovirus 1a (Kim et al., 1989) and rhinovirus 16 (Oliveira et al., 1993) (but not rhinovirus 14 [Rossmann et al., 1985]), and is now commonly referred to as "pocket factor." The pocket also is the binding site for a family of antiviral drugs that bind the particles by displacing the natural pocket factor (Smith et al., 1986; Grant et al., 1994; Hiremath et al., 1994). Binding of these drugs abolishes virion infectivity by preventing conformational changes that are required for productive cell entry. The binding of such drugs also has been shown to stabilize virions and empty capsids against thermally induced transitions from the native (N-antigenic) state to the heated (H-antigenic) state (Caliguiri et al., 1980; Rombaut et al., 1991). The presence of a ligand in this pocket thus has been proposed to play a critical role in regulating particle stability.

The interface between 5-fold related protomers has been shown to be a focal point for second-site mutations that suppress the temperature sensitivity of the P3/Sabin vaccine strain (Filman et al., 1989). This interface is analogous to an interface in a structurally related plant virus that is disrupted when the virions undergo a well-characterized expansion at alkaline pH (Robinson & Harrison, 1983), and it has been suggested that this interface might play a critical role in conformational transitions of poliovirus as well.

The N-terminal network forms a number of intraprotomer, intrapentamer, and interpentamer interactions that are expected to contribute significantly to the stability of capsid proteins and assembly products at every stage of the assembly process. This includes the folding of the capsid proteins to form protomers, the association of protomers into pentamers, and the association of pentamers into larger structures. Studies of the nontemperature-sensitive revertants of P3/Sabin have identified mutations in this network, indicating that the network is likely to play a role in virion stability. These mutation sites include residue 18 in the N-terminal extension of VP2 and residue 54 in the N-terminal extension of VP1 (Macadam et al., 1991). The mutation in VP2 is located in the 2-stranded β-sheet near the N-terminus VP2. Efforts to explain the effect of this mutation on temperature sensitivity led to the description of the 7-stranded interpentamer β-sheet. In addition, the proximity of this portion of VP2 to the N-terminus that is released upon VP0 cleavage led to the suggestion that the formation of this structure might be coupled to VP0 cleavage. The failure to form this critical interaction between pentamers completely would readily explain the dissociability of the empty capsids into pentamers upon exposure to mildly alkaline pH, and would also contribute to their thermal instability (Flore et al., 1990). The role of the VP1 mutation was not as readily interpreted.

The structure of the empty capsids shows unequivocally that neither the binding pocket nor the interface between 5-fold related protomers is significantly different from that in the mature virus. Thus, the structures of the ligand and its binding pocket are indistinguishable in mature virions and empty capsids. Similarly, considering only the cores and exterior loops of the capsid proteins, the structure of the interface between 5-fold related protomers in the virions and empty capsids is nearly identical. In contrast, much of the N-terminal network is absent in the empty capsid. This suggests that the complete formation of the network may depend on VP0 cleavage and/or RNA encapsidation. Although the failure to form portions of the network, and especially the interpentamer β-sheet, was anticipated (Flore et al., 1990), the extent to which the network is missing is surprising. The disorder of the entire N-terminal extension of VP1 and the observation that the missing portions of the network included a number of intraprotomer interactions (in addition to interprotomer and interpentamer interactions) is particularly surprising. We and others had come to consider the structure of the virion as a hierarchical system in which the final structure of the protomer is established early and then not altered, and in which the conformational alterations of assembled particles produce changes only in the interprotomer and interpentamer interfaces. The failure to find these intraprotomer interactions in the empty capsids has compelled us to reevaluate those assumptions.

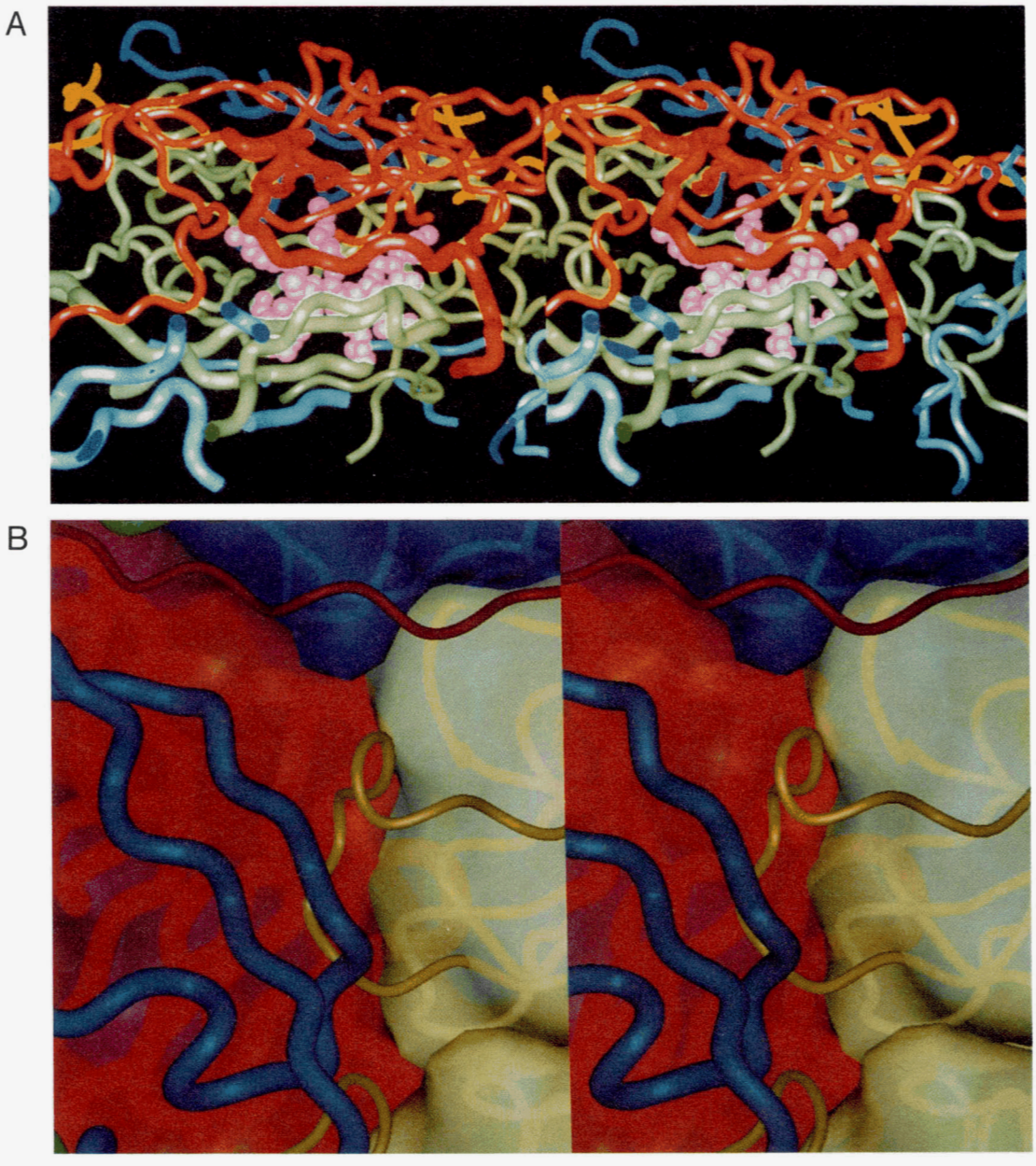

Fig. 7. *Caption appears on facing page.*

Among the intraprotomer interactions that are missing in the empty capsids, the contact provided by residue 44–56 of VP1, in the loop that underlies the cores of VP2 and VP3, is particularly provocative. This loop appears to buttress the otherwise tenuous association of VP2 and VP3 within a single protomer, and its importance has been shown by an increasingly large volume of mutational data. Specifically, residues in this loop have been found to be mutated in nontemperature-sensitive revertants of P3/Sabin (Macadam et al., 1991), in mouse-adapted strains of P1/Mahoney (Moss & Racaniello, 1991; Couderc et al., 1993; Guedo et al., 1994), and in strains of P3/Sabin selected for resistance to the antiviral drug disoxaril (Mosser et al., 1994), which binds in the core of VP1. In each case, the effect of the mutation can be rationalized as a compensation for an excessive destabilizing or stabilizing effect elsewhere. Furthermore, the mouse adaptation and drug resistance caused by mutations at this site suggest that, in addition to being important in the final steps of assembly, this site may play a critical role in regulating the conformational alterations associated with cell entry. These alterations are known to result in the externalization of VP4 and of most or all of the N-terminus of VP1. Thus, it might be necessary to disrupt the interactions of residues 44–56 in VP1 before VP4 and the N-terminus of VP1 can be externalized. Alternatively, in the event that alterations or disruption of the interface between VP2 and VP3 (within an individual protomer) is required, then mutations in this loop would play a critical role in regulation the conformational change. In either case, the mature virus can be viewed as a metastable intermediate link-

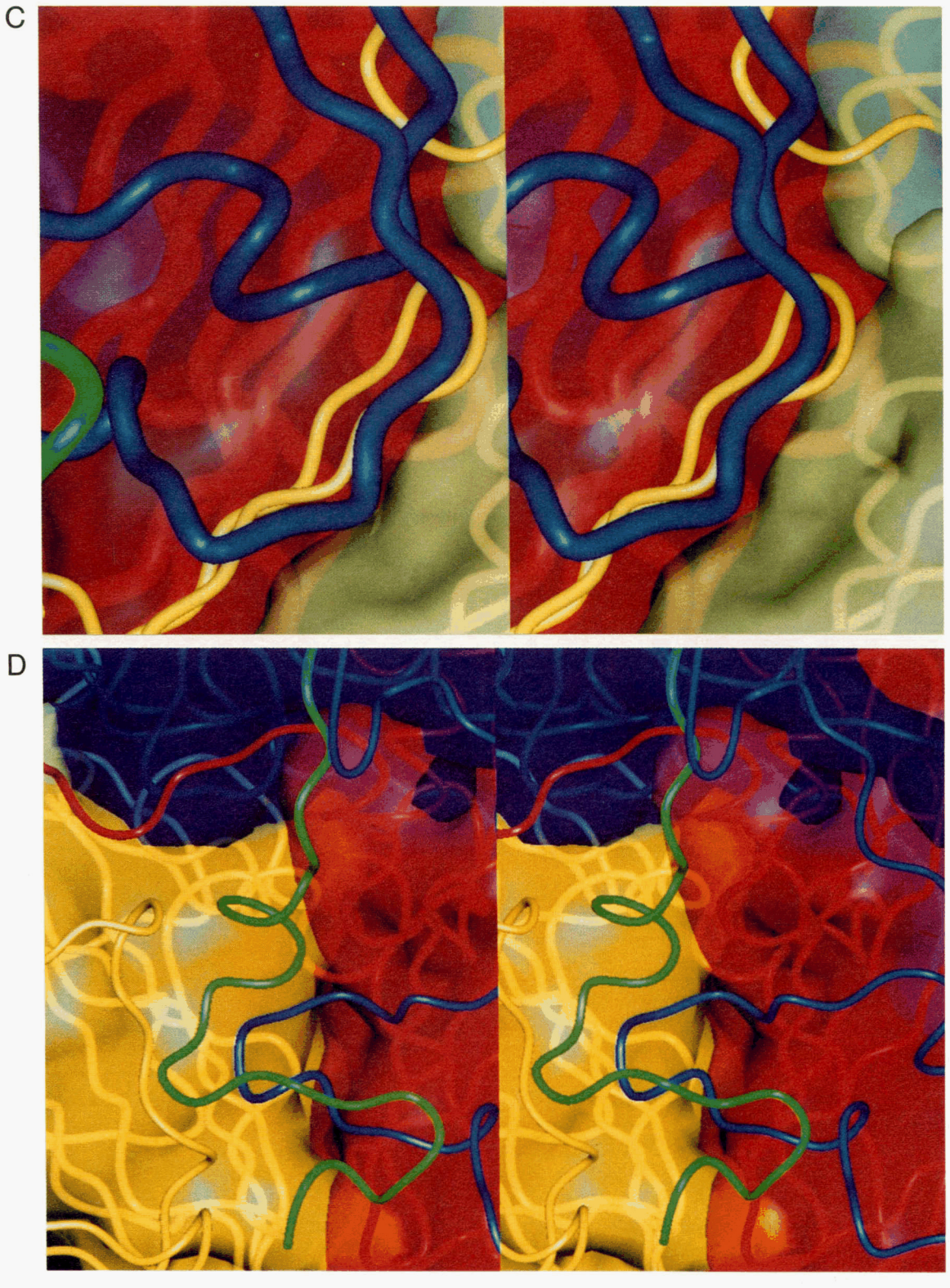

Fig. 7. Views of the major interactions made by the N-terminal arm of VP1. The panels correspond to the regions indicated in Figure 6. The coding is the same as that used in Figure 6. **A:** Interactions near the 5-fold axis. Residues 6–10 of VP1 provide 1 strand in a 3-stranded β-sheet that flanks a β-annular structure formed by the N-termini of VP3. The myristate groups covalently attached to the VP0/VP4 N-termini are shown in magenta. **B:** Residues 62–67 of VP1 make extensive contacts with residues 42–52 of VP2 from a 5-fold related protomer. **C:** Residues 36–38 of VP1 in the reference protomer provide a β-strand in an interpentamer 7-stranded β-sheet. Two β-strands are provided by VP2 from a 3-folded pentamer. The remaining 4 strands consist of the C, H, E, and F strands of VP3 in the reference protomer. **D:** Residues 44–56 of VP1 fill in a depression observed in the inner surface of the empty capsid by resting against the cores of VP2 and VP3. The loop of VP1 is itself overlaid by a segment of VP4. This figure was made using InsightII and Smooth_Surfer. (*Continued from facing page.*)

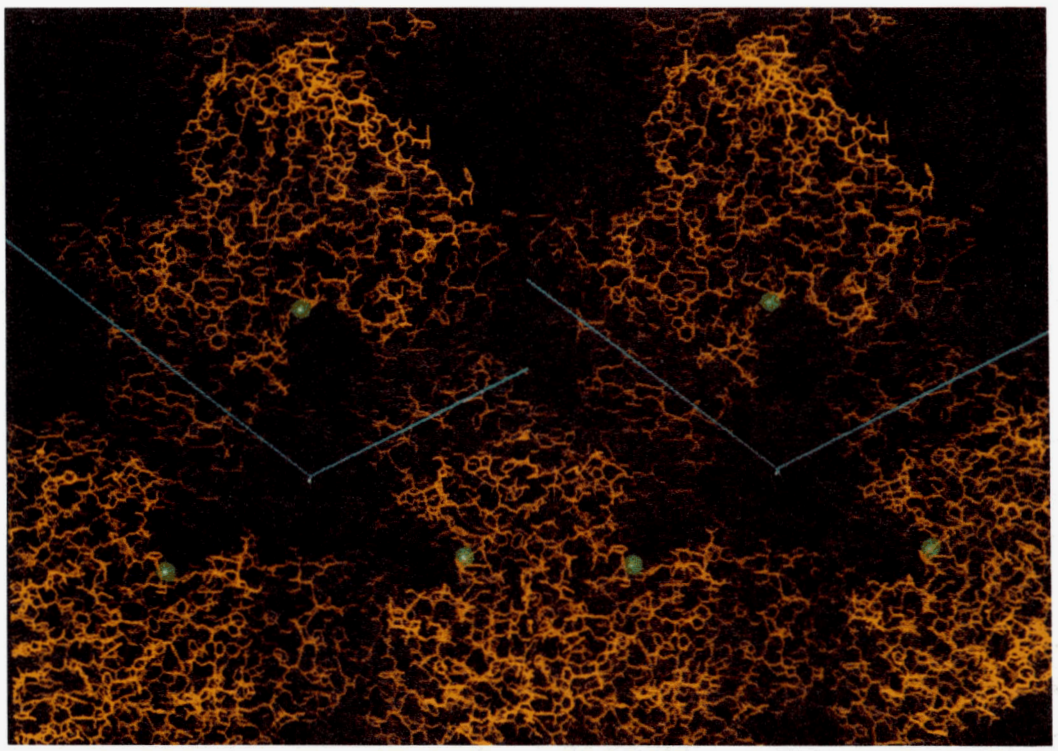

Fig. 8. A large trefoil-shaped depression in the inner surface of the empty capsid and centered on a 3-fold axis. Three 3-fold related protomers are shown. The blue lines indicate the approximate boundary of 1 pentamer. In the mature virus, this depression is filled in by the N-terminal extensions of VP1. The scissile bond, indicated in green, is situated on the rim of the depression. The figure was prepared using InsightII.

ing the final stages of assembly and early events of cell-entry pathway. In such a model, the primary role of the maturation cleavage of VP0 is to lock the mature virus in its metastable conformation.

Mechanism of VP0 cleavage

Another major goal of the structural studies of the empty capsids was to investigate the mechanism of VP0 cleavage. As stated previously, it is not clear whether the conformation of the scissile bond as it is seen in the empty capsid is directly relevant to cleavage or whether alterations in the structure, perhaps induced by encapsidation of viral RNA, are required before VP0 cleavage can take place. In either case, the empty capsid structure provides the only known structure for VP0 prior to its cleavage and provides a useful comparison with the structure of the mature virion for formulating hypotheses that may be tested by mutagenesis experiments. In the empty capsid structure, the fragment of VP0 that includes the scissile bond runs across the top of the trefoil-shaped depression that is centered on the particle 3-fold axis (Fig. 8). Several unusual features of this site may provide important clues to the mechanism of VP0 cleavage. First, a search was conducted for side chains that might participate in catalyzing the hydrolysis of the peptide bond. This search revealed that the stretch of VP0 spanning the scissile bond is located in the immediate vicinity of a histidine side chain (residue 195) from a highly conserved segment of VP2 (Fig. 9). The histidine residue and the residues on either side of it (Pro 194 and Glu 196) are absolutely invariant in all known picornavirus sequences, and the structure in the immediate vicinity of these residues is strikingly similar in all published picornavirus structures. In every case, the Pro at VP2:194 locks the main chain into a tight turn that allows the carbonyl oxygen of VP2:193 to make a hydrogen bond with the imidazole side chain of His 195. This hydrogen bond would be expected to increase density of negative charge on the nitrogen on the other side of the imidazole side chain. Second, the refined electron density maps for the empty capsid clearly contain density for 2 solvent molecules (presumably water) (Fig. 10) located immediately between the histidine side chain (VP2:195) and the scissile bond (Figs. 9, 10). Although neither of these "water" molecules is in contact with the scissile bond, either one could move into the appropriate position immediately below the carbonyl carbon should the C–O bond become more polarized. A small shift of the side chain of His 195 would bring it into a position where it could abstract a proton from the water in this activated complex. Third, the conformation of the main chain of VP0 in the immediate vicinity of the scissile bond is fairly unusual in that the carbonyl oxygen of the scissile bond and the carbonyl oxygen of the immediately following residue are both pointing in the same direction on the ridge of the trefoil-shaped depression. These 2 oxygen atoms are oriented to coordinate an ion or even a nucleotide base. Binding of such a ligand would increase the partial positive charge on the carbonyl carbon of the scissile bond.

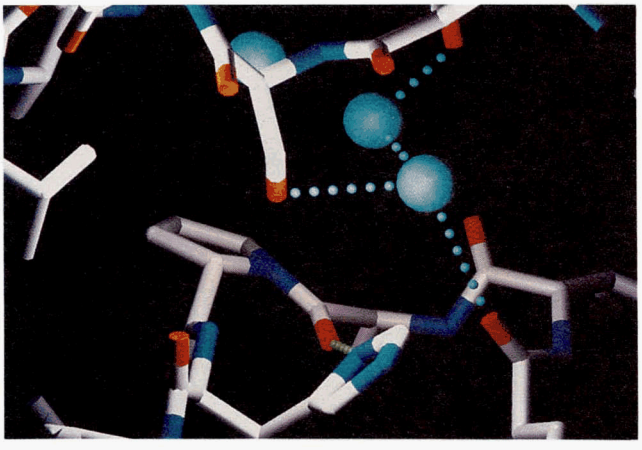

Fig. 9. The neighborhood of the scissile bond in the empty capsid. The scissile bond is the peptide bond in the upper half of the figure. Below it are shown 2 residues (Pro 194 and His 195) in a triplet of residues absolutely conserved among sequenced picornaviruses. The proline imposes a tight turn on the main chain and allows the imidazole side chain to form a hydrogen bond with main-chain carbonyl oxygen of residue 193. This interaction is found in all known picornavirus structures. Several ordered solvent molecules (represented as the large spheres) are observed in the vicinity. The small spheres indicate potential hydrogen bond interactions. This figure was created using SETOR.

Fourth, the hydrophobic character of the residues at the base of the depression below the scissile bond is consistent with the possibility that this site may bind other macromolecules that could participate in the catalytic mechanism. Obvious candidates would include the protease 3CD or the viral RNA. Although there is no evidence for macromolecules binding to this site, the trefoil-shaped depression is strikingly similar to a site in bean pod mottle virus (BPMV) that binds an ordered segment of the viral RNA (Chen et al., 1989) (Fig. 11). In fact, model-building experiments demonstrate that the RNA from the published coordinates of BPMV readily can be docked to this site with only minimal adjustments. If the corresponding site in poliovirus does bind RNA, there are at least 2 possible ways in which RNA binding could complete the catalytic machinery for VP0 cleavage. The first is that a base from the RNA coordinates the 2 carbonyl oxygens, thereby polarizing the scissile bond. The second, and perhaps more likely, possibility is that a phosphate from the RNA backbone may coordinate a metal ion (such as Zn^{2+}) and position it such that it coordinates the 2 carbonyl oxygens and thus polarizes the scissile bond. In either case, the structure of the catalytic site would become unstable subsequent to VP0 cleavage. Rearrangement of the newly released N-terminus of VP2 and C-terminus of VP4 would permit the disordered N-terminal extension of VP1 to fill the depression and eliminate the putative binding sites for the RNA and the "catalytic" waters.

Nucleation of assembly

The remarkable discovery of a feature in the empty capsid structure with obvious similarities to a known RNA-binding site in a structurally related virus raises the possibility that the binding of RNA on the inner surface of the empty capsid also may serve to nucleate assembly. Based on the structure of the empty capsid, a hypothetical model can be proposed in which the assembly of 3 pentamers around a 3-fold axis creates the trefoil-shaped depression that preferentially binds a specific sequence in the genome that has an unusually high affinity for this site. The "nucleation" site on the RNA might occur anywhere in the genome, but teleological arguments would suggest that the presence of the nucleation signal at the extreme 5′-end of the plus-

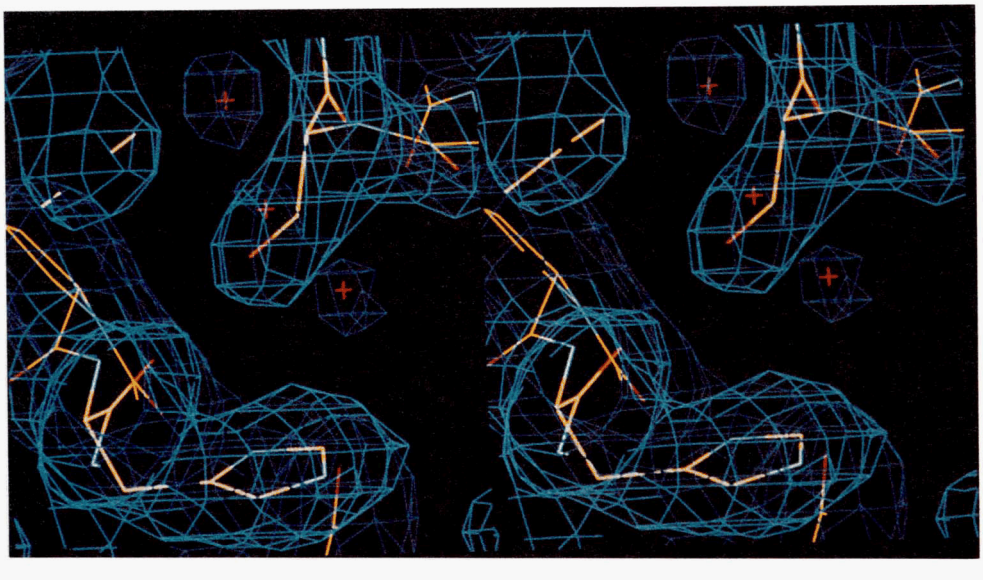

Fig. 10. Electron density corresponding to the region near the scissile bond. The scissile bond is near the top of the figure and the conserved histidine residue (residue 195 of VP2) is in the lower foreground. The density for nearby ordered solvent molecules is also seen. The electron density was obtained after imposing the phase constraints resulting from the noncrystallographic symmetry. This figure was created using FRODO.

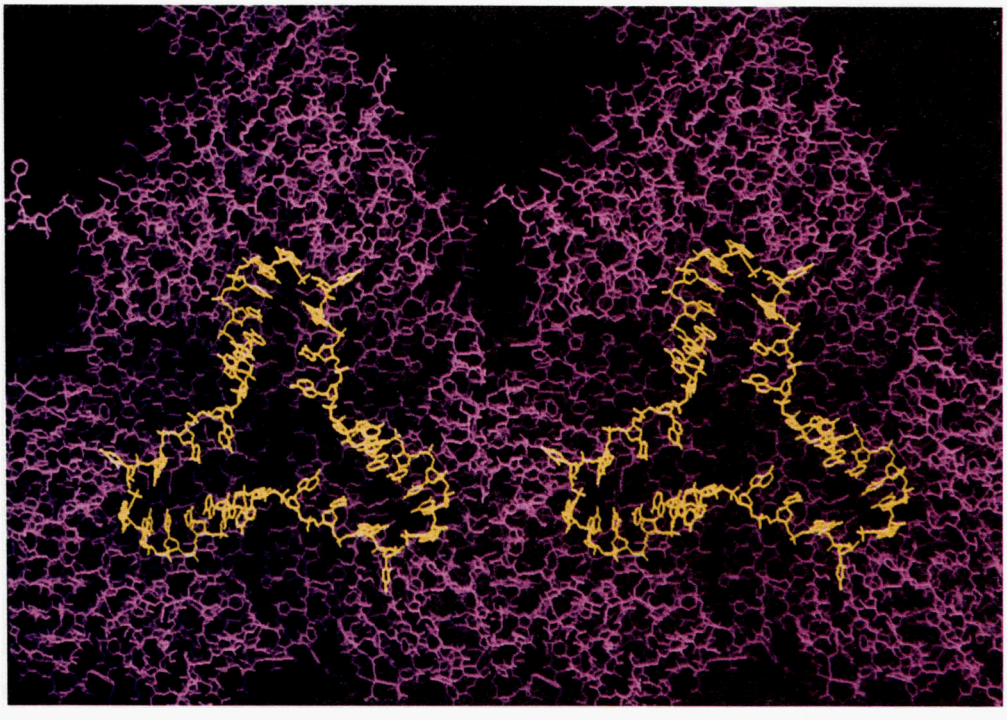

Fig. 11. The inner surface of the bean pod mottle virus (Chen et al., 1989). Three 3-fold related protomers are shown in approximately the same perspective as that in Figure 8. The ordered RNA seen in this structure is shown in yellow. Removal of the RNA in a graphics display reveals a depression that is very similar in size and form to that observed in the poliovirus empty capsid. This figure was created using InsightII.

strand RNA might be most efficient. This would provide a convenient method for committing a nascent strand of plus-sense RNA to become a genomic RNA, rather than a message RNA or a template for minus-sense RNA synthesis. The switch to commit to genomic RNA would depend on the accumulation of a sufficient level of assembly-competent pentamers. An attractive candidate for the nucleation site is the tRNA-like structure that is predicted to occur at the 5′-end of the genome-sense RNA. Recent studies have shown that this loop also binds to the viral protein 3CD and to a host protein (Andino et al., 1993) and suggest that the binding of these proteins plays a key role in the initiation of plus-strand synthesis. One or both of these proteins also might be required for the formation of the nucleation complex. Such a requirement would account for recent observations that the production of infectious virus in an in vitro translation system depends on the de novo synthesis of genomic RNA (Molla et al., 1991). Subsequent growth might proceed through the addition of pentamers to this nucleation complex in a fashion that is highly analogous to the proposed mechanism for the assembly of plant viruses such as turnip crinkle virus (Harrison et al., 1987). In such a model, cleavage of VP0 might depend on the assembly of an intact catalytic site including the capsid proteins and viral RNA. If RNA actually is required for cleavage, the cleavage mechanism must be able to accommodate a variety of RNA sequences (in addition to the preferred nucleation sequence) in the later stages of assembly in order to account for the experimental observation that there are at most 1–2 copies of VP0 per virion in most virus preparations. Such cleavage would "lock in" correctly assembled complexes. Incorrectly assembled complexes would remain uncleaved and free to dissociate. The cleavage of VP0 might occur either concurrently with assembly or following completion of assembly, but it must proceed slowly relative to the speed of pentamer addition to account for the failure of VP2 and VP4 to accumulate in structures other than mature virions.

Materials and methods

Virus

Seed stocks of the Mahoney strain of type 1 poliovirus (P1/Mahoney) were obtained from Marie Chow (MIT). The stock was a low-passage inoculum prepared from a plaque isolated from a transfection of HeLa cells with an infectious cDNA clone of the P1/Mahoney genome (Racaniello & Baltimore, 1981).

Preparation of empty capsids

Empty capsids were prepared by infection of HeLa cells with P1/Mahoney in the presence of guanidine-HCl. In a typical empty capsid preparation, 12 L of log-phase cells at a density of 3.5–4.5 $\times$ 10^5 cells/mL were pelleted and resuspended at a density of approximately 4 $\times$ 10^7 cells/mL in Hanks' balanced salt solution (Gibco BRL) supplemented with 2 mM L-glutamine, 2.5 mM Hepes (pH 7.0), 1$\times$ vitamins (from 100$\times$ MEM vitamin solution, Gibco BRL), 1$\times$ penicillin/streptomycin (from

200× penicillin/streptomycin, Gibco BRL), 1 mg/L $MgCl_2$, and 1 mg/L $MgSO_4$ (infection medium) at room temperature. Virus was attached to cells by adding P1/Mahoney at a multiplicity of infection of 10 plaque-forming units per cell, and the attachment was allowed to proceed at room temperature for 30 min with constant gentle mixing. Infection was initiated by diluting this mixture to a cell density of 3.5–4.5 × 10^6 cells/mL with prewarmed (37 °C) infection medium supplemented with 2% fetal bovine serum and allowed to proceed at 37 °C. Virus proteins were labeled by adding 500 μCi of ^{3}H-leucine (1 mCi/mmol) (Amersham) at 2.75 h postinfection, and RNA synthesis was stopped by adding guanidine-HCl to a concentration of 200 μg/mL at 3.5 h postinfection. At 5 h postinfection, the cells were pelleted by centrifugation and washed once with cold phosphate-buffered saline (PBS). From this point on in the purification, the empty capsids were maintained at 4 °C. The cells were lysed by treating with ice-cold 1% NP-40 detergent in RSB buffer (10 mM Tris, 10 mM NaCl, 1.5 mM $MgCl_2$, pH 6.3, at room temperature). The cell debris was pelleted by centrifuging for 15 min at 400 × *g* and the supernatant was collected. Then viral and subviral particles in the supernatant were pelleted into a 40% sucrose cushion by centrifuging 5.5 h at 140,000 × *g*. The material in the cushion was thoroughly resuspended, transferred to a Beckman Quick-Seal centrifuge tube, and brought to a volume of 5 mL with RSB buffer. Five milliliters of 80% Nycodenz in RSB (w/v) were then added and the entire mixture was repeatedly inverted to make the mixture uniformly 40% in Nycodenz. The mixture was centrifuged for at least 8 h at 400,000 × *g* at 4 °C in a vertical rotor to allow sufficient development of the self-forming Nycodenz gradient. The gradient was then fractionated into 350-μL aliquots. The specific radioactivity of each fraction was counted to locate the empty capsid peak. The fractions containing this peak were pooled and run through a Bio-Rad desalting column to exchange the empty capsids into RSB buffer without Nycodenz. Empty capsid particles then were pelleted by centrifugation at 350,000 × *g* for 2.5 h. The pellets were allowed to soak overnight in approximately 400 μL RSB, then resuspended and layered onto a 15–30% sucrose gradient in RSB. The gradient was centrifuged 4 h at 270,000 × *g* and then fractionated in 400-μL aliquots. Fractions containing the empty capsids were located by counting the radioactivity of each fraction. These were pooled and concentrated either by pelleting or using a microconcentrator. Purity of the sample was assessed by SDS-PAGE with silver staining using the Pharmacia Phast system. Protein concentration was determined using the Pierce BCA protein assay kit.

Assay for alkaline dissociability

The alkaline dissociability of empty capsid samples was tested by adding an equal volume of 0.1 M Tris base to the sample and incubating on ice for 10 min. The pH of the sample was then neutralized by adding about a 10× volume of PBS. This sample was loaded onto a 12-mL 15–30% sucrose density gradient in PBS and centrifuged for 3 h at 270,000 × *g*. The gradient was fractionated into 20-mL scintillation vials (500 μL/fraction). The samples were mixed with 1 mL H_2O, followed by 16 mL of EcoScint A scintillation fluid, and counted.

Crystallization and data collection

Crystals of empty capsids were grown by dialyzing 5–15 μL samples of empty capsid (~15 mg/mL) initially in 0.8 M NaCl, PMC7 (10 mM Pipes, 5 mM $MgCl_2$, 1 mM $CaCl_2$, pH 7.0) buffer against 0.05 M NaCl, PMC7 at 4 °C. The empty capsid crystallizes in space group $P2_12_12$, with half a virus particle per asymmetric unit. The unit cell dimensions are a = 322.9 Å, b = 358.0 Å, c = 380.1 Å. Prior to data collection, crystals were transferred into 25% ethylene glycol (v/v) in PMC7 buffer so that the crystal could be cooled to −12 °C without freezing the mother liquor. The crystals were mounted in quartz capillaries with no attempt to orient the crystal in any particular setting. Diffraction data were collected using the Cu-Kα radiation from an Enraf-Nonius GX-13 rotating-anode generator operating at 40 kV, 60 mA, with Franks mirror optics. Oscillation data were recorded on CEA Reflex 25 film. During each exposure, the crystal was oscillated over a 0.5° range, and exposure times were typically 3–4 h. The films were digitized on a 50-μ raster using an Optronics PixelGetter scanner. The crystal orientations were estimated using an autoindexing algorithm (T.O. Yeates & D.J. Filman, unpubl.) and refined. The diffraction data were integrated and processed by filtering to remove background and by deconvolution (D.J. Filman, unpubl.). Partially recorded reflections were corrected to their fully recorded equivalents by a local implementation of the postrefinement method (Winkler et al., 1979). Reflections recorded with partiality of 50% or greater were merged to assemble the final data set from 51 0.5° oscillation photographs.

Structure determination

Initial phases for the empty capsid diffraction data were obtained by molecular replacement using the refined structure of the mature P1/Mahoney poliovirus structure as a phasing model. Dissimilarities between the empty capsid and the mature P1/Mahoney virion were identified by difference Fourier maps. These regions were pruned from the model. Phase refinement by application of the 30-fold noncrystallographic symmetry constraints was initiated using the pruned Mahoney model. The empty capsid model was built into the constrained electron density map using the computer graphics program FRODO (Jones, 1985). In ensuing rounds of phase refinement, the most current empty capsid model was used. The model was initially refined alternating cycles of pseudo-real-space refinement (Grant et al., 1992), application of noncrystallographic symmetry constraints, and manual rebuilding. In the latter stages of refinement, the pseudo-real-space refinement procedure was replaced by a recently developed procedure that calculates the changes in atomic position by combining the gradient derived from the X-ray term with the gradient from the stereochemical energy term (D.H. Jacobson, J.M. Hogle, & D.J. Filman, in prep.). As in the pseudo-real-space refinement procedure, the gradient of the X-ray term is estimated from the slope of a vector difference map (thus reflecting the difference between the current model and that portion of the symmetry-constrained electron density that encloses a single protomer). The contribution of the stereochemical term to the gradient is obtained by a small number of steps of energy minimization using the X-PLOR stereochemical potential (Brün-

ger, 1992). In each cycle, shifts from these 2 terms are suitably weighted and then added to obtain the shifts to be applied to the model. As before, the refinement proceeded by alternating rounds of automated model refinement, imposition of phase constraints, and manual rebuilding of the model. Portions of the structure unique to the empty capsid were added to the model as they became evident in the averaged map. Most of the empty capsid structure that eventually was built was fairly well defined after the first round of phase averaging.

Acknowledgments

This work was supported by NIH grant AI20566 (to J.M.H.) and in part by an NIH postdoctoral fellowship (AI08780-03) to R.B., a NATO fellowship (SA.5-2-05(CRG.900033)) to O.F., and a grant from the Keck Foundation to establish a structural biology facility in the Department of Biological Chemistry and Molecular Pharmacology. The authors thank Dr. Ann Mosser (University of Wisconsin-Madison) for sharing data prior to publication.

References

Acharya R, Fry E, Stuart D, Fox G, Rowlands D, Brown F. 1989. The three-dimensional structure of foot-and-mouth disease virus at 2.9 Å resolution. *Nature 337*:709–716.

Andino R, Rieckhof GE, Achacoso PL, Baltimore D. 1993. Poliovirus RNA-synthesis utilizes an RNP complex formed around the 5′-end of viral RNA. *EMBO J 12*:3587–3598.

Arnold E, Luo M, Vriend G, Rossmann MG, Palmenberg AC, Parks GD, Nicklin MJ, Wimmer E. 1987. Implications of the picornavirus capsid structure for polyprotein processing. *Proc Natl Acad Sci USA 84*:21–25.

Bricogne G. 1974. Geometric sources of redundancy in intensity data and their use in phase determination. *Acta Crystallogr A 30*:395–405.

Brünger AT. 1992. *X-PLOR (version 3.1): A system for X-ray crystallography and NMR*. New Haven, Connecticut: Yale University Press.

Caliguiri LA, McSharry JJ, Lawrence GW. 1980. Effect of arildone on modifications of poliovirus in vitro. *Virology 105*:86–93.

Chen Z, Stauffacher C, Ynge L, Schmidt T, Bomu W, Kamer G, Shanks M, Lomonossoff G, Johnson JE. 1989. Protein–RNA interactions in an icosahedral virus at 3.0 Å resolution. *Science 245*:154–168.

Compton SR, Nelsen B, Kirkegaard K. 1990. Temperature-sensitive mutant fails to cleave VP0 and accumulates provirions. *J Virol 64*:4067–4075.

Couderc T, Hogle J, Le Blay H, Horaud F, Blondel B. 1993. Molecular characterization of mouse-virulent poliovirus type 1 Mahoney mutants: Involvement of residues of polypeptides VP1 and VP2 on the inner surface of the capsid protein shell. *J Virol 67*:3808–3817.

Evans SV. 1993. SETOR: Hardware lighted three-dimensional solid model representations of macromolecules. *J Mol Graphics 11*:134–138.

Fernandez-Tomas CB, Baltimore D. 1973. Morphogenesis of poliovirus. II. Demonstration of a new intermediate, the provirion. *J Virol 12*:1181–1183.

Filman DJ, Syed R, Chow M, Macadam AJ, Minor PD, Hogle JM. 1989. Structural factors that control conformational transitions and serotype specificity in type 3 poliovirus. *EMBO J 8*:1567–1579.

Flore O, Fricks CE, Filman DJ, Hogle JM. 1990. Conformational changes in poliovirus assembly and cell entry. *Semin Virol 1*:429–438.

Ghendon Y, Yakobson E, Mikhejeva A. 1972. Study of some stages of poliovirus morphogenesis in MiO cells. *J Virol 10*:260–266.

Grant RA, Filman DJ, Fujinami R, Icenogle JP, Hogle JM. 1992. Three-dimensional structure of Theiler's virus. *Proc Natl Acad Sci USA 89*: 2061–2065.

Grant RA, Hiremath CN, Filman DJ, Syed R, Andries K, Hogle JM. 1994. The three-dimensional structure of poliovirus complex with capsid-stabilizing anti-viral drugs. *Curr Biol 4*:784–797.

Guedo N, Couderc T, Calvez I, Hogle J, Colbere-Garapin F, Blondel B. 1994. Substitutions in the capsid of poliovirus type 1 mutants selected in neuroblastoma cells confer a neurovirulent phenotype in mice to the Mahoney strain. *J Virol*. Forthcoming.

Guttman N, Baltimore D. 1977. Morphogenesis of poliovirus. IV. Existence of particles sedimenting at 150S having the properties of provirions. *J Virol 23*:363–367.

Harbor JJ, Bradley J, Anderson CW, Wimmer E. 1991. Catalysis of poliovirus VP0 maturation cleavage is not mediated by serine 10 of VP2. *J Virol 65*:326–334.

Harrison SC, Sorger PK, Stockley PG, Hogle J, Altman R, Strong RK. 1987. Mechanism of RNA virus assembly and disassembly. In: Brinton MA, Rueckert RR, eds. *Positive strand RNA viruses*. New York: Alan R. Liss, Inc. pp 379–395.

Hiremath CN, Grant RA, Filman DJ, Hogle JM. 1994. The binding of the antiviral drug WIN 51711 to the Sabin strain of type 3 poliovirus: Structural comparison with drug binding in rhinovirus 14. *Acta Crystallogr*. Forthcoming.

Hogle JM, Chow M, Filman DJ. 1985. Three-dimensional structure of poliovirus at 2.9 Å resolution. *Science 229*:1358–1365.

Holland JJ, Kiehn ED. 1968. Specific cleavage of viral proteins as steps in the synthesis and maturation of enteroviruses. *Proc Natl Acad Sci USA 60*:1015–1022.

Icenogle J, Gilbert SF, Grieves J, Anderegg J, Rueckert RR. 1981. A neutralizing monoclonal antibody against poliovirus, its reaction with virus related antigens. *Virology 115*:211–215.

Jacobson MF, Baltimore D. 1968a. Morphogenesis of poliovirus . I. Association of the viral RNA with coat protein. *J Mol Biol 33*:369–378.

Jacobson MF, Baltimore D. 1968b. Polypeptide cleavages in the formation of poliovirus proteins. *Proc Natl Acad Sci USA 61*:77–84.

Jacobson MF, Baltimore D. 1970. Further evidence on the formation of poliovirus proteins. *J Mol Biol 49*:657–669.

Jones TA. 1985. Interactive computer graphic: FRODO. *Methods Enzymol 115B*:157–171.

Kim S, Smith TJ, Chapman MS, Rossmann MG, Pevear DC, Dutko FJ, Felock PJ, Diana GD, McKinlay MA. 1989. Crystal structure of human rhinovirus serotype 1A (HRV1A). *J Mol Biol 210*:91–111.

Luo M, He C, Toth KS, Zhang CX, Lipton HL. 1992. Three-dimensional structure of Theiler murine encephalomyelitis virus (BeA strain). *Proc Natl Acad Sci USA 89*:2409–2413.

Luo M, Vriend G, Kamer G, Minor I, Arnold E, Rossmann MG, Boege U, Scraba DG, Duke GM, Palmenberg AC. 1987. The atomic structure of Mengo virus at 3.0 Å resolution. *Science 235*:182–191.

Macadam AJ, Ferguson G, Arnold C, Minor PD. 1991. An assembly defect as a result of an attenuating mutation in the capsid proteins of the poliovirus type 3 vaccine strain. *J Virol 65*:5225–5231.

Marongiu ME, Pani A, Corrias MV, Sau M, LaColla P. 1981. Poliovirus morphogenesis. I. Identification of 80S dissociable particles and evidence for artifactual production of procapsids. *J Virol 39*:341–347.

Minor PD, Dunn B, Evands DMA, Magrath DI, John A, Howlett J, Phillips A, Westrup G, Wareham K, Almond JW, Hogle JM. 1989. The temperature sensitivity of the Sabin type 3 vaccine strain poliovirus: Molecular and structural effects of a mutation in the capsid protein VP3. *J Gen Virol 70*:1117–1123.

Molla A, Paul AV, Wimmer E. 1991. Cell-free, de novo synthesis of poliovirus. *Science 254*:1647–1651.

Moss EG, Racaniello VR. 1991. Host range determinants on the interior of the poliovirus capsid. *EMBO J*:1067–1074.

Mosser AG, Sgro JY, Rueckert RR. 1994. Distribution of drug-resistance mutations in type 3 poliovirus identifies three regions involved in uncoating functions. *J Virol*. Forthcoming.

Oliveira MA, Zhao R, Lee WM, Kremer MJ, Minor I, Rueckert RR, Diana GD, Pevear DC, Dutko FJ, McKinlay MA, Rossmann MG. 1993. The structure of human rhinovirus 16. *Structure 1*:51–68.

Oppermann H, Koch JG. 1973. Kinetics of poliovirus replication in HeLa cells infected by isolated RNA. *Biochem Biophys Res Commun 52*: 635–640.

Pallansch MA, Kew U, Semler BL, Omilianowski DR, Anderson CW, Wimmer E, Rueckert R. 1984. Protein processing map of poliovirus. *J Virol 49*:873–880.

Palmenberg AC. 1982. In vitro synthesis and assembly of picornaviral capsid intermediate structures. *J Virol 44*:900–906.

Palmenberg AC. 1990. Proteolytic processing of picornaviral polyprotein. *Annu Rev Microbiol 44*:603–623.

Phillips BA, Fennel R. 1973. Polypeptide composition of poliovirions, naturally occurring empty capsids, 14S precursor proteins. *J Virol 12*: 291–299.

Phillips BA, Summers DF, Maizel JV Jr. 1968. In vitro assembly of poliovirus related proteins. *Virology 35*:216–226.

Racaniello VR, Baltimore D. 1981. Cloned poliovirus complementary DNA is infectious in mammalian cells. *Science 214*:916–919.

Rickwood D. 1983. Properties of iodinated density-gradient media. In: Rickwood D, ed. *Iodinated density gradient media*. Oxford, UK: IRL Press, Ltd. pp 1–21.

Robinson IK, Harrison SC. 1983. The structure of the expanded state of tomato bushy stunt virus at 8 Å resolution. *Nature 297*:563–568.

Rombaut B, Andries K, Boeyé A. 1991. A comparison of WIN 51771 and R 78206 as stabilizers of poliovirus virions and procapsids. *J Gen Virol 72*:2153–2157.

Rombaut B, Vrijsen R, Brioen P, Boeyé A. 1982. A pH-dependent antigenic conversion of empty capsids of poliovirus studied with the aid of monoclonal antibodies to N and H antigen. *Virology 122*:215–218.

Rossmann MG, Arnold E, Erickson JW, Frankenberger EA, Griffith JP, Hecht HJ, Johnson JE, Kamer G, Luo M, Mosser Ag, Rueckert RR, Sherry B, Vriend G. 1985. Structure of a human common cold virus and functional relationships to other picornaviruses. *Nature 317*:145–153.

Smith TJ, Kremer MJ, Luo M, Vriend G, Arnold E, Kamer G, McKinlay MA, Diana GD, Otto MJ. 1986. The site of attachment in human rhinovirus 14 for antiviral agents that inhibit uncoating. *Science 233*:1286–1293.

Watanabe Y, Watanabe K, Katagiri K, Hinuma Y. 1965. Virus-specific proteins produced in HeLa cells infected with poliovirus: Characterization of a subunit-like protein. *J Biochem 57*:733–741.

Winkler FK, Schutt CE, Harrison SC. 1979. The oscillation method for crystals with very large unit cells. *Acta Crystallogr A 35*:901–911.